



HAL
open science

Characterization of the microstructure of dairy systems using automated image analysis

Juliana V.C. Silva, David Legland, Chantal Cauty, Irina Kolotuev, Juliane
Floury

► **To cite this version:**

Juliana V.C. Silva, David Legland, Chantal Cauty, Irina Kolotuev, Juliane Floury. Characterization of the microstructure of dairy systems using automated image analysis. *Food Hydrocolloids*, 2015, 44, pp.360-371. 10.1016/j.foodhyd.2014.09.028 . hal-01130408

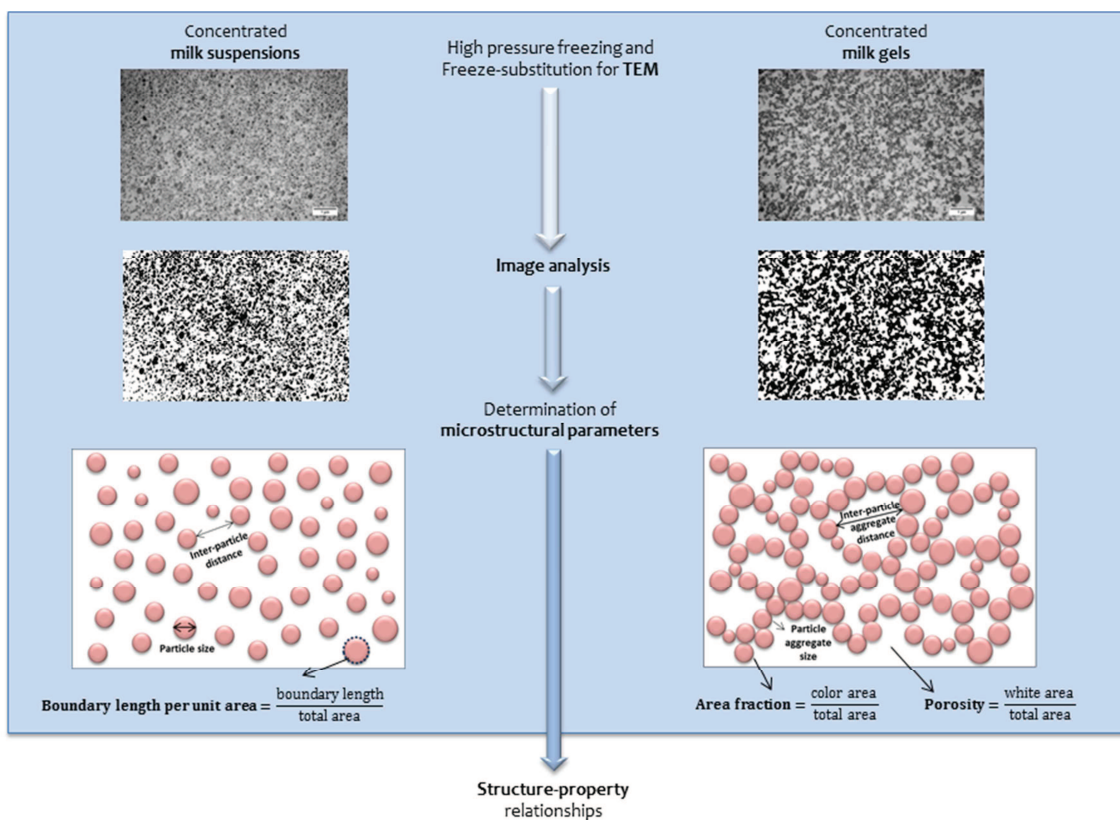
HAL Id: hal-01130408

<https://univ-rennes.hal.science/hal-01130408v1>

Submitted on 11 Mar 2015

HAL is a multi-disciplinary open access archive for the deposit and dissemination of scientific research documents, whether they are published or not. The documents may come from teaching and research institutions in France or abroad, or from public or private research centers.

L'archive ouverte pluridisciplinaire **HAL**, est destinée au dépôt et à la diffusion de documents scientifiques de niveau recherche, publiés ou non, émanant des établissements d'enseignement et de recherche français ou étrangers, des laboratoires publics ou privés.



ACCEPTED MANUSCRIPT

1 Characterization of the microstructure of dairy systems using automated image analysis

2
3 **Juliana V. C. Silva^a, David Legland^{b,c,d,e}, Chantal Cauty^a, Irina Kolotuev^{f,g}, Juliane**
4 **Floury^{a,h,*}**

5 ^aINRA, UMR1253 Science and Technology of Milk and Eggs, F-35042 Rennes, France

6 ^bINRA, UMR782 Food Process Engineering and Microbiology, F-78850 Thiverval-Grignon,
7 France

8 ^cAgroParisTech, UMR782 Food Process Engineering and Microbiology, F-78850 Thiverval-
9 Grignon, France

10 ^dINRA, UMR1318 Institut Jean-Pierre Bourgin, F-78026 Versailles, France

11 ^eAgroParisTech, Institut Jean-Pierre Bourgin, F-78026 Versailles, France

12 ^fMRic-TEM, UMS3480 Microscopy Rennes Imaging Center, F-35043 Rennes, France

13 ^gIGDR, UMR6290 University of Rennes 1, 2, F-35043 Rennes, France

14 ^hAgrocampus Ouest, UMR1253 Science and Technology of Milk and Eggs, F-35042 Rennes,
15 France

16
17 ¹Corresponding author: Juliane Floury

18 Telephone number: +33 (0)2 23 48 54 52; Fax number: +33 (0)2 23 48 55 78

19 E-mail: juliane.floury@agrocampus-ouest.fr

27 **ABSTRACT**

28 A sound understanding of the microstructure of dairy products is of great importance in order
29 to predict and control their properties and final quality. The aim of this study was to develop
30 an automated image analysis procedure to characterize the microstructure of different dairy
31 systems. A high pressure freezing coupled with freeze-substitution (HPF-FS) protocol was
32 applied prior to transmission electron microscopy (TEM) in order to minimize any
33 modification of the microstructure of the dairy systems investigated. The developed image
34 analysis procedure was first validated on synthetic images of suspensions, and then on two
35 types of concentrated milk suspensions. Microstructural data relating to casein micelles in
36 milk suspensions were taken from the literature. The established procedure was then applied
37 to the two corresponding rennet-induced milk gels, prepared from the same milk concentrates
38 used for suspensions preparation. The automated image analysis procedure allowed the
39 reliable estimation of several characteristic microstructural parameters including area fraction,
40 porosity, boundary length per unit area, particle aggregate size, inter-particle aggregate
41 distance and tortuosity. The relative ease of estimating these microstructural parameters from
42 the automated image analysis method could make it useful for routine measurements of milk
43 gels. Moreover, the method enabled a useful discrimination between two different types of
44 milk gels. This novel approach can contribute to a better understanding of the effects of
45 processing on the structure-property relationships in dairy products, and may be applied to
46 other food systems.

47

48

49 **Keywords:** Transmission electron microscopy, microstructure, dairy systems, milk gels,
50 freeze-substitution, quantitative image analysis

51

52 1. Introduction

53

54 The microstructure is one of the major determining factors of flavor, physicochemical
55 and of the functional properties of dairy products. Thus understanding the microstructure of
56 dairy products during their manufacture and subsequent storage is of great importance in
57 order to predict and control their properties and final quality (Gunasekaran & Ding, 1999; El-
58 Bakry & Sheehan, 2014).

59 Dairy products are principally based on caseins, which make up 80% of the protein in
60 milk. Around 95% of the caseins in milk exist as large colloidal particles between 50 and 600
61 nm in diameter (mean ~120 nm), which are known as “casein micelles” (Fox & Brodkorb,
62 2008). The microstructure of dairy products depends principally on the organization of these
63 casein micelles that can change as a function of the technological treatment applied to milk.
64 For instance, casein micelles are easily destabilized by adding rennet to milk to form a rennet-
65 induced gel, the basis of cheese making (Lucey, 2002; Dalgleish & Corredig, 2012). In
66 contrast to milk, where caseins are present in suspension, milk gels form a continuous three
67 dimensional network whose properties greatly depend on the microstructure.

68 The microstructure of dairy products is commonly investigated using instrumental
69 techniques such as light or electron microscopy techniques. Light microscopy, such as
70 Confocal Laser Scanning Microscopy (CLSM), allows the observation of dairy products with
71 a minimum of sample preparation and with a resolution up to 0.25 microns (Fenoul, Le
72 Denmat, Hamdi, Cuvelier, & Michon, 2008; Morand, Guyomarc'h, Legland, & Famelart,
73 2012; Ercili-Cura et al., 2013). By using this technique, it may be possible to distinguish the
74 structure of the milk gel, but not the fine organisation of casein micelles that form its
75 microstructure. Electron microscopy provides a resolution at a nanometer scale, making it
76 possible to observe the organization of the gel protein network itself. Scanning Electron

77 Microscopy (SEM) has already been used for investigating the microstructure of a variety of
78 dairy products (Marchesseau, Gastaldi, Lagaude, & Cuq, 1997; McMahon, Fife, & Oberg,
79 1999; Fallico et al., 2006; Le Feunteun & Mariette, 2007; 2008). However, SEM provides
80 only a topographical view of the sample surface, making it difficult to quantify properties
81 from the observed images. On the other hand, Transmission Electron Microscopy (TEM)
82 provides observation of a slice of the sample, making it possible to investigate its internal
83 structure. This can provide a basis for the quantitative description of the sample
84 microstructure (Reis & Malcata, 2011).

85 Conventional TEM preparation procedures include chemical fixation, dehydration and
86 embedding, which are frequently problematic in samples with high water content. Such
87 methods can introduce numerous artifacts that alter the relationships that exist between the
88 structural components (Kalab, Allan-Wojtas, & Mistry, 1995). Therefore, the use of low-
89 temperature methods, such as freeze-fracture replication (Büchheim, 1982; McMahon &
90 McManus, 1998), freeze-substitution (Goff, Verespej, & Smith, 1999; Smith, Kakuda, &
91 Goff, 2000), cryo-TEM (Waninge, Nylander, Paulsson, & Bergenstahl, 2003; 2004) and high
92 pressure freezing coupled with freeze-substitution methods (Ramasubramanian, Webb,
93 D'Arcy, & Deeth, 2013) are preferable in order to preserve the original structure of the dairy
94 sample ahead of the conventional TEM.

95 Nowadays, qualitative interpretations of micrographs are often no longer enough.
96 Image analysis is necessary to also provide quantitative data for the analysis and design of
97 food microstructure (Aguilera, Stanley, & Baker, 2000). Such image analysis has been
98 recently introduced into dairy research for a wide range of applications (Wium, Pedersen, &
99 Qvist, 2003; Impoco, Carrato, Caccamo, & Tuminello, 2006; Rovira, Lopez, Ferrandini, &
100 Laencina, 2011; Geng, van den Berg, Bager, & Ipsen, 2011; Ong, Dagastine, Kentish, & Gras,
101 2011; 2012; 2013).

102 Micrograph images of dairy samples can be quantified through the morphometry of
103 individual objects or particles (Gunasekaran & Ding, 1999; Rovira et al., 2011; Impoco, Fucà,
104 Pasta, Caccamo, & Licitra, 2012; Fucà, Pasta, Impoco, Caccamo, & Licitra, 2013). When a
105 protein network cannot be easily segmented, gray level texture analysis can be used to discern
106 the variations of gray levels from confocal images (Fenoul et al., 2008; Morand et al., 2012;
107 Ercili-Cura et al., 2013). An alternative to particle-based image analysis and image texture
108 analysis is the characterization of protein network as a binary microstructure. This method
109 consists of quantifying geometrical properties of a structure that cannot be described by a set
110 of individual particles, but rather as a complex structure with voids and branches that is
111 observed in a representative window. While this approach is common in materials science
112 (Ohser & Mücklich, 2000) and for describing porous media (Torquato, 2002), to the authors'
113 knowledge no attempt have been made to quantify the microstructure of dairy products.

114 The aim of this work was thus to develop an automated image analysis procedure to
115 characterize the microstructure of dairy systems. The proposed procedure comprised the
116 automated segmentation of the protein network from TEM micrographs, and the subsequent
117 computation of microstructural parameters by assimilating the protein network to a porous
118 media. The high pressure freezing and freeze-substitution (HPF-FS) protocol was used in
119 order to minimize modification of the microstructure of dairy systems during sample
120 preparation for TEM. Microstructural parameters considered in this study included global
121 morphological parameters (area fraction, porosity, boundary length per unit area), binary
122 image granulometry, that measures the typical sizes of particles (or of particle aggregates or
123 of voids), and a tortuosity parameter that describes the microstructure at a larger scale.
124 Tortuosity is a parameter mainly related to mass transfer properties and has been measured in
125 several porous media such as rocks, sediments, soil, zeolites, biological tissues, etc. (Suman &
126 Ruth, 1993; Latour, Kleinberg, Mitra, & Sotak, 1995; Zalc, Reyes, & Iglesia, 2004; Wu, van

127 Vliet, Frijlink, & van der Voort Maarschalk, 2006; Shen & Chen, 2007; Lanfrey, Kuzeljevic,
128 & Dudukovic, 2010). Some authors have also been applying the theory of porous media to
129 food systems and have been estimating tortuosity values from diffusion coefficients in food
130 media (Crossley & Aguilera, 2001; Sam Saguy, Marabi, & Wallach, 2005). The determination
131 of tortuosity directly from image analysis would therefore be of great interest for
132 understanding the diffusion phenomena in dairy products.

133 The concept of measuring the above listed parameters using image analysis was first
134 tested on a synthetic image representing a suspension of micelles as might be observed under
135 conditions similar to the present study. The image analysis method was subsequently
136 validated on two concentrated milk suspensions of similar casein concentration, but produced
137 by different methods. Microstructural data relating to casein micelles in milk suspensions
138 were taken from the literature for validation. The method was then applied to the
139 corresponding concentrated milk gels, obtained by rennet-induced coagulation of the same
140 milk concentrates used for suspensions preparation, in order to show a wider application of
141 this procedure.

142

143 **2. Material and Methods**

144

145 *2.1. Preparation of concentrated milk suspensions and gels*

146

147 Two concentrated milk suspensions and two concentrated milk gels presenting similar
148 casein composition were produced. These dairy systems were based on two different protein
149 milk concentrates produced using either Microfiltration (MF) or Ultrafiltration (UF)
150 processes.

151

152 *2.1.1. MF concentrate*

153 The aim of the membrane filtration process developed in this study was to obtain an
154 almost pure casein concentrate, dispersed in the same aqueous phase of milk, in order to
155 mimic as much as possible the protein composition of a real cheese. Skim milk (Entremont,
156 Montauban de Bretagne, France) was initially filtered to remove contaminating bacteria using
157 the microfiltration pilot equipment GP7 fitted with a 0.8 μm Sterilox GP membrane. This
158 microfiltrate was then concentrated by microfiltration using a 0.1 μm aluminum Zircone
159 membrane. This smaller pore size allowed the concentration of the casein fraction only, the
160 size of the whey proteins in milk being sufficiently small to cross the membrane. In order to
161 increase the concentration factor of the caseins, it was necessary to proceed to a diafiltration
162 step of the concentrate, using the MF permeate instead of water in order to keep the same
163 aqueous phase of milk in the final concentrate. The permeate had been previously
164 ultrafiltered with a 5 kD membrane to remove the whey proteins. The overall filtration
165 process allowed concentrating the total proteins of milk by a factor of 4.3. Neither NaCl nor
166 cream was added, leaving a non-salty and a non-fatty MF concentrate. The composition of the
167 MF concentrate (pH 6.6) is given in Table 1.

168

169 *2.1.2. UF concentrate*

170 The UF concentrate was produced following previously described procedures (Ulve et
171 al., 2008; Silva, Peixoto, Lortal, & Flourey, 2013). Unlike microfiltration, the ultrafiltration
172 process allowed the concentration of all the proteins of milk, both the caseins and the whey
173 proteins. This UF concentrate has then the same protein composition as for some commercial
174 cheeses obtained by using the MMV technology, such as Pavé d’Affinois (Maubois, Mocquot,
175 & Vassal, 1969; Maubois & Mocquot, 1971; Maubois & Mocquot, 1975). Overall, the total
176 proteins of milk were concentrated in this case by a factor of 5. Once again, neither NaCl nor

177 cream was added, leaving a non-salty and a non-fatty UF concentrate. The composition of the
178 UF concentrate (pH 6.6) is given in Table 1.

179 The MF concentrate was used without further preparation whereas the UF concentrate
180 was heated at 93°C for 15 min (Aly et al., 2011) and then cooled using melting ice for 3 min.
181 Sodium azide was added to both the MF and heat-treated UF concentrates at a final
182 concentration of 0.05% (wt/wt) in order to prevent microorganism growth. About 1 mL of the
183 MF concentrate or of the heat-treated UF concentrate were poured into 2 mL Eppendorf tubes
184 and then incubated at 30°C for 1 h and then held at 19°C for 2 h to obtain the MF-suspension
185 or the UF-suspension, respectively. Both suspensions were passively aspirated by using
186 cellulose microcapillary tubes with a 200 µm inner diameter ahead of further preparation for
187 TEM.

188 The concentrated milk gels were produced from the same concentrates (i.e.; MF or
189 heat-treated UF concentrates). In this case, after adding sodium azide to the concentrates
190 (0.05% wt/wt), the coagulant agent Maxiren 180 (DSM Food Specialties, Seclin, France) was
191 added giving a final concentration of 0.03% (v/v). After homogenization, 600 µL of each
192 mixture (MF or heat-treated UF concentrate + coagulant agent) was slowly poured into mini-
193 gel cassette® systems (IFR Norwich, U.K.), containing flat gold-plated specimen carriers (0.5
194 mm thick, 1.5 mm in diameter, 200 µm deep; Leica Cat #16706898). The gel cassettes®
195 systems were incubated at 30°C for 1 h to enable coagulation and then at 19°C for 2 h to
196 obtain the final gels based on each concentrate.

197

198 2.2. *Transmission electron microscopy*

199

200 The prepared concentrated milk suspensions and gels were frozen using a Leica EM
201 PACT2 high-pressure freezer (Leica Microsystems, Vienna, Austria). The sample carriers,

202 cellulose microcapillary tubes or flat gold-plated specimen carriers, were pre-coated with 1%
203 phosphatidylcholine (Sigma-Aldrich Ltd.) diluted in chloroform to avoid sample sticking. No
204 cryo-protecting agent was added to the samples. For the freeze-substitution step, Leica EM
205 AFS2 freeze substitution machine (Leica Microsystems, Vienna, Austria) was used. The
206 frozen samples were transferred in liquid nitrogen to a processing container equipped with a
207 flat spacer (Leica Microsystems, Vienna, Austria). The frozen samples were freeze-
208 substituted in 2% osmium tetroxide diluted in anhydrous acetone. After an initial incubation
209 of 8h at -90°C the temperature was gradually ($5^{\circ}\text{C}/\text{hour}$) raised to -30°C and samples were
210 then left for another 8h at this temperature. The solvent-fixative solution was replaced with
211 pre-chilled mix of ethanol 3:1 resin (epon-araldite mix; Sigma-Aldrich Ltd). The temperature
212 was then gradually brought up to room temperature and further ethanol:resin substitutions
213 were done following the resin manufacturer instructions. Thin sections (90 nm) of embedded
214 samples were cut with a diamond knife using a Reichert ultramicrotome. The sections were
215 contrasted with 4% aqueous solution of uranyl acetate and observed using a JEM-1400
216 Transmission Electron Microscope (JEOL Ltd., Tokyo, Japan) operated at 120 kV
217 accelerating voltage. Digital images were acquired using the Gatan SC1000 Orius[®] CCD
218 camera (4008 x 2672), set up with the imaging software Gatan DigitalMicrograph[™] (Gatan,
219 Pleasanton, USA).

220 Several TEM micrographs were taken on different parts of two independent samples
221 of each of the four dairy systems. Ten micrograph images were chosen independently for each
222 dairy system for further image analysis.

223 The resulting images each represented an area of $9.97 \times 6.64 \mu\text{m}$ and showed the
224 microstructure of the samples at a magnification of $\times 20000$. Images were saved as 32-bit
225 grayscale dm3 images of 4008×2670 pixels (where 1 pixel = 2.5 nm).

226

227 2.3. *Image processing of TEM micrographs*

228

229 Several image processing steps were necessary to automatically segment the TEM
230 images of the four dairy systems (concentrated milk suspensions and gels). These steps are
231 schematically set out in Fig. 1. Each image was normalized using a blank background image
232 (obtained without sample or resin) (Fig. 1B). This permitted the removal of intensity
233 variations over the image. Histogram normalization procedure was applied and the result was
234 converted to images based on 256 shades of gray (Fig. 1C). As artifacts could be detected on
235 some micrographs, they were removed by applying a “black top-hat” operation with a square
236 structuring element of 200x200 pixels (Fig. 1D). Black top-hat is a tool (taken from
237 mathematical morphology) that enhances dark structures smaller than the chosen structuring
238 element while removing larger variations (Soille, 2003). A smoothing operator was then
239 applied (by computing the average of pixel values in a circular neighborhood with radius of
240 10 pixels) to remove the acquisition noise (Fig. 1E). The two phases were contrasted, with
241 images histograms showing two peaks (Fig. 1F). “Otsu automated threshold” is commonly
242 used for the segmentation of dairy product images (Ong et al., 2011; Hussain, Grandison, &
243 Bell, 2012; Impoco et al., 2006) and was used for the segmentation in the present study. Otsu
244 threshold consists in identifying the threshold value that best discriminates between the two
245 phases, by minimizing the intra-class variance while maximizing inter-class variance (Otsu,
246 1979). The segmentation procedure was validated by visual inspection of the binary images
247 superimposed on the original images.

248 2.4. Quantification of microstructural parameters

249

250 The values of the microstructural parameters determined in the present work may
251 depend on several factors such as sample thickness and image processing (i.e., filter choice,
252 segmentation threshold). Therefore, the proposed image analysis procedure was first validated
253 by comparing microstructural parameters of concentrated milk suspensions with those of both
254 synthetic images and data taken from the literature. Finally, the values of microstructural
255 parameters obtained for the different dairy systems in the same conditions could be compared
256 between them.

257

258 2.4.1. Generation of synthetic images of a suspension

259 In order to validate and help to interpret microstructural parameters, the developed
260 image analysis method was applied on synthetic images mimicking a theoretical suspension
261 of micelles. A set of non-overlapping balls was generated in a 3D cuboid with dimensions
262 $5 \times 5 \times 2 \mu\text{m}$. The diameter of the balls was chosen as 120 nm, corresponding to the mean
263 diameter of casein micelles (Fox & Brodtkorb, 2008). In order to avoid edge effects, a margin
264 of 200 nm was applied on all sides. The number of balls was chosen to have a numerical
265 density equal to $160 \text{ micelles}/\mu\text{m}^3$, corresponding to an expected number of 8000 within the
266 cuboid. This value was chosen to generate an area fraction in the synthetic images similar to
267 the one observed for milk suspensions in the present study. To avoid overlap, a minimal
268 distance of 130 nm was imposed between the micelle centers. The physical cut was
269 represented by a horizontal slice with thickness 90 nm, and located in the middle of the
270 cuboid. An example of a synthetic suspension of micelles is shown on Fig. 2A. The
271 intersection of the slice with the set of balls was used to generate a planar binary image
272 representing a virtual observation of the model system. A resolution of 2.5 nm by pixel was

273 used, resulting in a 2000x2000 pixels binary image (Fig. 2B). Ten images were thus generated
274 to address the variability of measurement method. Due to the thickness of the slice, some
275 micelles seemed to overlap, seemingly forming small agglomerates. Other micelles present a
276 smaller section because they were not located within the sampled slice. Matlab software was
277 used both to simulate the 3D synthetic suspensions and to generate the corresponding binary
278 images (Mathworks, Natick, MA). The Free-D software was used to produce the sample
279 image of Fig. 2A (Andrey & Maurin (2005), <http://free-d.versailles.inra.fr/html/freed.html>).

280

281 *2.4.2. Global morphometry*

282 Global morphometry was used to determine three global microstructural parameters:
283 area fraction, porosity, and boundary length per unit area. If the sampling slice can be
284 assumed to have a small thickness relative to size of the structures, these parameters can be
285 directly related to 3D properties of the network by using stereological relations.

286 Area fraction was defined as the ratio between dark area (i.e.; the protein matrix) with
287 respect to the total area of the image. The dark area corresponds to the area covered by
288 particles (for suspensions) or by particle aggregates (for gels) in the micrograph cross-
289 sections. Porosity is the complementary parameter and can be defined as the division of the
290 void area by the total image area. In the binary image, porosity was calculated as white area
291 (free space, corresponding to the aqueous phase) as a percentage of the total area (Impoco et
292 al., 2006; Rovira et al., 2011).

293 The boundary length per unit area is the length of the perimeter around all the particle
294 edges or boundaries (for suspensions) or particle aggregate edges or boundaries (for gels),
295 divided by the total image area. The boundary length per unit area thus measures the quantity
296 of interface between the protein phase and the aqueous phase. For a comparable area density,
297 its value will be larger for systems with small structures and/or tortuous interfaces, and

298 smaller for systems with large structures and/or smooth interfaces. Boundary length was
 299 estimated by using a discretized version of Crofton formula, which consists in counting the
 300 number of intercepts with lines of various orientations, and normalized by the area of the
 301 image (Ohser & Mücklich, 2000; Legland, Kiêu, & Devaux, 2007).

302

303 2.4.3. Image morphological granulometry

304 The typical size of particles (or particle aggregates) and inter-particle (or inter-particle
 305 aggregate) distances were determined by applying binary image granulometry on the
 306 segmented images. Binary image granulometry is based on image transformations depending
 307 on the size of a mask referred to as a “structuring element”. One of the basic transformations
 308 (taken from mathematical morphology) is the morphological opening, which effectively
 309 removes objects smaller than the structuring element (Soille, 2003). By applying openings of
 310 increasing sizes to the dairy system images, the particles (or particle aggregates) are
 311 progressively removed. The complementary transformation is morphological closing, which
 312 effectively makes the voids smaller than the defined structuring element disappear. Following
 313 the same process, applying closings of increasing size to the images leads to a progressive
 314 elimination of the part of the image showing the voids in the structure. Thus, by either
 315 method, a particle (or void) size distribution curve is produced.

316 The curve $V(i)$ is generated by counting the number of pixels after each closing or
 317 opening step. This is then normalized according to the initial and final number of pixels
 318 $V(initial)$ and $V(final)$ and the finite difference is computed to build a granulometric curve:

319

$$g(i) = \frac{V(i) - V(i + 1)}{V(initial) - V(final)} \quad (1)$$

320

321 In the current study, the largest size (diameter) of the disk structuring element was 121
 322 pixels, corresponding to about 300 nm on the image. To reduce computation time, structuring
 323 element diameters were considered with a step of 4 pixels. To compare granulometric curves
 324 for a set of samples, each granulometric curve was summarized by computing its geometric
 325 mean. The following weighted sum was used:

326

$$m = \exp\left(\sum_{i=1}^{imax} g(i) * \log(t_i)\right) \quad (2)$$

327

328 where $g(i)$ is the percent of grey level variation for the step i , t_i is the size of the structuring
 329 element in μm and $imax$ is the number of closing/opening steps (Legland, Devaux, Bouchet,
 330 Guillon, & Lahaye, 2012). The geometric means of the granulometric curves obtained with
 331 the openings procedure were interpreted as the average size of particles (for suspensions) or
 332 particle aggregates (for gels). The geometric means of the granulometric curves obtained with
 333 the closings procedure were interpreted as the average size of the aqueous phase between the
 334 particles or particle aggregates.

335 A schematic representation of microstructural parameters determined for suspensions
 336 and gels by using the image morphological granulometry method is given in Fig. 3.

337

338 2.4.4. Tortuosity

339 The tortuosity in every point in the aqueous phase can be defined as the ratio of the
 340 shortest path (i.e.; avoiding the protein network) between two opposing borders of the image,
 341 over the Euclidean distance between the same borders (Delarue & Jeulin, 2003; Wu et al.,
 342 2006). An illustration of the tortuosity for a sample structure is given in Fig. 4. The 3D
 343 tortuosity cannot be determined from 2D images, but 2D tortuosity can be used to

344 quantitatively compare the microstructure of different dairy systems observed under similar
345 conditions.

346 For points belonging to aqueous phases totally included in the protein network, no
347 path can be defined to image borders. Consequently, the tortuosity over an image was defined
348 as the average value measured at points for which shortest paths could be computed. As the
349 length of the shortest path is always greater than the Euclidean distance, the tortuosity is
350 always greater than or equal to one. The tortuosity value increases with the complexity of the
351 protein network separating the aqueous phase.

352 In order to assess the variability of the tortuosity measurement, each image was
353 divided into four sub-images, and tortuosity was calculated for each sub-image. For most
354 images, the tortuosity of the complete image was similar to the average value of the sub-
355 images (the difference being less than the standard deviation). However, for some images, the
356 difference was greater, due to large blocks of protein network that introduce a large variability
357 in the measurement.

358

359 *2.5. Software implementation*

360

361 Image processing and analysis was performed using Fiji-win64 processing software.
362 The quantification of morphological features required the development of specific plugins,
363 which are available on request from the authors, or from the Internet at [http://www.pfl-
365 cepia.inra.fr/index.php?page=ijGeodesics_en](http://www.pfl-
364 cepia.inra.fr/index.php?page=ijGranulometry_en), [http://www.pfl-](http://www.pfl-
366 cepia.inra.fr/index.php?page=imMinkowski_en)

367

368

369 2.6. Statistical Analysis

370

371 The mean values of microstructural parameters obtained for the four different dairy
372 systems studied (MF-suspension, UF-suspension, MF-gel and UF-gel) were statistically
373 compared using R software (version R i386 3.0.2) (R Foundation for Statistical Computing,
374 Vienne, Austria). Results are presented with the mean value and the standard deviation. One-
375 way analysis of variance (ANOVA) and Tukey's paired comparison test were applied in order
376 to determine which means are significantly different from one another at the 95% family-wise
377 confidence level. The Student's test was applied in order to compare the two suspensions and
378 the two gels.

379

380 3. Results and Discussion

381

382 3.1. Image processing of TEM micrographs

383

384 Sample images of TEM acquisition obtained by using the HPF-FS protocol are
385 presented in Fig. 5, for both pairs of suspensions and gels. The dark phase corresponds to the
386 protein matrix (i.e.; particles or particle aggregates). The lighter phase corresponds to the
387 aqueous phase, formed by water, lactose, minerals and free amino acids. In all dairy systems,
388 the particles and particle aggregates were homogeneously distributed.

389 The particle aggregates observed in the gels (Fig. 5C and 5D) are larger compared to
390 the individual particles in suspensions (Fig. 5A and 5B).

391 Representative segmented TEM micrographs of the concentrated milk suspensions and
392 gels are illustrated in Fig. 6. These segmented images correspond to the TEM micrographs
393 shown in Fig. 5. The black phase of the segmented micrographs corresponds to the protein

394 matrix (i.e.; particles or particle aggregates), while the white phase corresponds to the
395 aqueous phase.

396

397 *3.2. Quantification of microstructural parameters*

398

399 *3.2.1. Validation of the automated image analysis procedure*

400 Microstructural parameters were measured for the two concentrated milk suspensions
401 in order to validate the image processing of TEM micrographs by comparing with values
402 taken from the literature. Obtained values were also compared to those obtained on synthetic
403 suspension images. Table 2 presents the values of the microstructural parameters obtained
404 from TEM micrographs of the milk suspensions.

405 Area fractions measured from TEM micrographs were equal to 0.34 ± 0.02 and $0.33 \pm$
406 0.01 for the MF- and UF-suspensions, respectively. Area fractions did not differ statistically
407 ($p < 0.05$) between the MF- and UF-suspensions. This fact can be explained by the same
408 casein concentration in both suspensions (130 g/kg).

409 The number of micelles in the synthetic suspension image was adjusted to obtain a
410 value of area fraction similar to that for the real suspensions. The related value for the
411 synthetic images was equal to 0.338 ± 0.005 . The other microstructural parameters can
412 therefore be compared between synthetic and real suspensions.

413 The mean particle size obtained by granulometry on the synthetic suspension images
414 was estimated as 116.3 ± 0.3 nm. This is very close to the diameter of the casein micelles,
415 validating the image analysis method in this respect. Nonetheless, the measured values on the
416 synthetic suspension images were still smaller than the real diameter of casein micelles, which
417 is attributed to the presence of smaller sections of micelles.

418 Fig. 7 shows granulometric curves for the milk suspensions representing the particle
419 size distribution (Fig. 7A and 7B for MF- and UF-suspensions, respectively) and the
420 distribution of inter-particle distances (Fig. 7C and 7D for MF- and UF-suspensions,
421 respectively). A good repeatability of the particle size distributions and of inter-particle
422 distance is noted for both MF- and UF-suspensions. The corresponding mean particle size and
423 inter-particle distance values from the geometric means are given in Table 2.

424 The mean particle size was 88 ± 3 nm and 99 ± 4 nm for the MF- and UF-suspensions.
425 At the casein concentration used (130 g/kg, corresponding to ~ 140 g/L for these suspensions),
426 casein micelles are fully separated from each other, i.e., below the concentration of random-
427 close packing estimated as ~ 178 g/L (Bouchoux, Debbou, Gésan-Guiziou, Famelart, &
428 Doublier, 2009). Casein micelles present in milk are known to have a broad size distribution
429 with diameters ranging from 50 to 500 nm, and a mean diameter of ~ 120 nm (Fox &
430 Brodkorb, 2008). The values obtained by image analysis fall within this range of diameters
431 found for casein micelles in unconcentrated milk, but are smaller than the indicated mean
432 diameter. Similar results were reported by Srilaorkul et al. (1991), who studied the effect of
433 skim milk ultrafiltration on particle size using conventional TEM. They measured particle size
434 by observation using a Baush and Lomb measurement magnifier, counting and classifying the
435 micelles into 10 classes, each with a width of 20 nm. They saw a decrease in mean casein
436 micelle diameter from 118 nm in normal milk to 87 nm in milk that had been concentrated
437 five times. The change in the composition of casein and minerals as a result of the
438 ultrafiltration of milk may be responsible for the change in average diameter of the casein
439 micelles.

440 The UF-suspension presented a mean particle size greater than that for the MF-
441 suspension. The larger mean particle size (of about 10 nm) for the UF-suspension may be due
442 to the association of denatured whey proteins on the surface of the micelles due to the heat

443 treatment applied to the UF concentrate (Jeurnink & de Kruif, 1993; Anema & Li, 2003; Nair,
444 Dalgleish, & Corredig, 2013). Anema & Li (2003) demonstrated that the diameter of casein
445 micelles in heated reconstituted skim milk increased by 19 nm as a consequence of heat
446 treatments. For the concentrated milk studied in the same work, prepared by subjecting milk
447 to a combination of ultrafiltration and microfiltration techniques, an overall increase of 5 nm
448 was observed when samples at pH 6.55 were heated for 45 min at 90°C. These values are
449 comparable to the increase of about 10 nm of mean particle size found in the current study for
450 the (heat-treated) UF-suspension.

451 The mean inter-particle distance obtained from the image analysis was 123 ± 5 nm and
452 132 ± 2 nm for the MF- and UF-suspensions, respectively. These values are smaller than
453 those predicted from the synthetic suspension (153 ± 3 nm). This may be explained by the
454 differences in the diameter distribution: as real suspensions contain a larger number of small
455 micelles the mean free distance will be less. The mean free distance between casein micelles
456 in unconcentrated milk is reported as around 240 nm (Fox & Brodkorb, 2008). As expected,
457 the mean inter-particle distances between the casein micelles would be smaller in the
458 concentrated milk suspensions than in milk (25 g/L) due to the higher casein concentration
459 (130 g/kg, i.e. around 140 g/L) as a result of the membrane technology (microfiltration or
460 ultrafiltration processes) applied. It is known that when the concentration of total solids in
461 skim milk increases (e.g. during ultrafiltration), the distance between the casein micelles
462 decreases due to the increased volume fraction (Karlsson, Ipsen, Schrader, & Ardö, 2005).

463 The images of the MF- and UF-suspensions presented similar area fraction values
464 whereas the particle size and inter-particle distance values were statistically different. The
465 mean inter-particle distance was greater for the UF-suspension (when compared with the MF-
466 suspension) that counteracted, to some extent, the effect of the larger mean particle size.

467 The MF-suspension images presented a boundary length per unit area of 13.3 ± 0.5
468 $\mu\text{m}/\mu\text{m}^2$, and the UF-suspension a value of $12.1 \pm 0.2 \mu\text{m}/\mu\text{m}^2$. This parameter is a measure of
469 the quantity of interface between the protein phase (black phase) and the aqueous phase
470 (white phase). For comparison, the values measured for the synthetic suspension images were
471 $11.5 \pm 0.2 \mu\text{m}/\mu\text{m}^2$. This may be explained by the fact that synthetic suspensions are more
472 regular than real ones. The value was significantly larger for the MF-suspension than for the
473 UF-suspension. This result may have been expected because a suspension with small particles
474 (MF-suspension) will have a greater interface (between the particles and the aqueous phase)
475 and thus a larger boundary length per unit area value. As both suspensions have the same area
476 fraction, the observed difference depends on the regularity of the interface. Assuming a
477 suspension of spherical particles, an interpretation is that the MF-suspension is composed of
478 smaller particles compared with the UF-suspension.

479 The tortuosity was 1.08 ± 0.01 for the MF-suspension and 1.06 ± 0.01 for the UF-
480 suspension. These values were not significantly different ($p < 0.05$) but they were a little bit
481 larger than that for the synthetic suspensions (1.043 ± 0.001). It can be observed that
482 tortuosity value increases when mean distance between micelles decreases, and when
483 boundary length per unit area increases.

484 Overall, the microstructural parameter values predicted for concentrated milk
485 suspensions by the image analysis procedure were in agreement with literature findings and
486 also with results obtained for a synthetic suspension. This fact allowed us to validate the
487 image processing of TEM micrographs.

488
489
490
491

492 3.2.2. *Application of the automated image analysis procedure to milk gels*

493 The image analysis procedure validated previously for the two types of concentrated
494 milk suspensions was then applied to their corresponding gels, which had been obtained by
495 rennet-induced coagulation, in order to determine their microstructural parameters.

496 The microstructure of milk gels is more complex than that for suspensions and
497 depends on several factors such as the type of coagulation and the treatment applied to the
498 milk concentrate prior to the coagulation step. It is well known that the addition of chymosin
499 cleaves a specific bond of the κ -casein on the surface of the micelles. This reduces the steric
500 and electrostatic repulsion between the micelles, and the destabilized micelles thus begin to
501 aggregate to form the gel (Mellema, Heesakkers, van Opheusden, & van Vliet, 2000).

502 Table 3 sets out the values for the microstructural parameters obtained from the TEM
503 images of MF- and UF-gels.

504 The mean area fractions were 0.49 ± 0.03 and 0.50 ± 0.02 for MF- and UF-gels,
505 respectively, which were significantly ($p < 0.05$) larger than the values obtained for the
506 related suspensions (0.34 ± 0.02 and 0.33 ± 0.01 for MF- and UF-suspensions, respectively).
507 However, similar area fraction values should be expected for concentrated milk suspensions
508 and gels presenting the same casein concentration. This unexpected result may be explained
509 by the aggregation of casein micelles in the gel which could induce changes in the apparent
510 density of particles on the TEM images, due to the slice thickness of the sample.

511 Curds from heat-treated milks tend to be weak, ragged in appearance with a poor
512 matting ability and poor fusion of the gel network, giving rise to more porous matrices (Singh
513 & Waungana, 2001). However, in the present study, the UF-gel (made from heat-treated UF
514 concentrate) presented the same porosity compared with the MF-gel (about 0.50). This fact
515 can be explained by the ultrafiltration of the milk prior to coagulation in the case of the UF-
516 gel. It is known that gels formed from UF concentrates are much firmer than the

517 corresponding curds produced from unconcentrated milks at comparable levels of β -
518 lactoglobulin denaturation and association (Singh & Waungana, 2001). This result is
519 interesting because gels obtained from different technological treatments but with the same
520 casein composition have a similar porosity. Thus, heat treatment in combination with
521 concentration processes such as ultrafiltration may yield opportunities to correct curd
522 properties.

523 Fig. 8 shows granulometric curves obtained by applying the opening procedure (Fig.
524 8A and 8B for MF- and UF-gels, respectively), representing the distribution of particle
525 aggregate sizes and by the closing procedure (Fig. 8C and 8D for MF- and UF-gels,
526 respectively), representing the distribution of inter-particle aggregate distances obtained from
527 TEM micrographs. Fig. 8 demonstrates the good repeatability of the distribution of particle
528 aggregate size and inter-particle aggregate distance values obtained from different TEM
529 micrographs of the MF- and UF-gels. Values for these same parameters are set out in Table 3.

530 The MF-gel exhibited a mean particle aggregate size of 141 ± 3 nm, slightly larger
531 than the mean particle aggregate size in UF-gel, 135 ± 8 nm. Concerning the rennet-induced
532 gels, it is known that in milk that has been heated, the κ -casein is broken down by chymosin
533 (as it is in unheated milk), but that the micelles do not aggregate well (Kethireddipalli, Hill, &
534 Dalgleish, 2011). This is due to the presence of denatured whey proteins on the micellar
535 surface, which may hinder the close approach of the potentially interacting sites on the
536 micelles (Dalgleish & Corredig, 2012). Waungana, Singh, & Bennett (1996) observed that the
537 denaturation of individual whey proteins and their association with the casein micelles
538 resulted in prolonged gelation times and reduced gel firmness in gels produced from heat-
539 treated UF milk (UHT system; 80°C to 140°C for 4s) due to the formation of a limited
540 number of reactive sites at the micellar surface. It may thus follow that the denatured whey
541 proteins associated on the micellar surface in the UF concentrate prevented the close approach

542 of casein micelles, resulting in smaller particle aggregates in the (heat-treated) UF-gel when
543 compared with the MF-gel.

544 As expected, the mean particle aggregate size is larger in the two gels studied
545 compared with the mean particle size in the corresponding suspensions. This may be
546 explained by the aggregation of casein micelles in gels as a consequence of the addition of the
547 coagulant agent (rennet) (Walstra, Bloomfield, Jason Wei, & Jenness, 1981).

548 Mean inter-particle aggregate distances were shown by image analysis as 147 ± 5 nm
549 for the MF-gel, significantly greater than the mean value of 131 ± 7 nm obtained for the UF-
550 gel. The MF-gel contained particle aggregates and inter-particle aggregate distances greater
551 than those found in the UF-gel. These results are consistent with the boundary length unit area
552 values obtained for these gels.

553 The boundary length per unit area for the UF-gel was $10.7 \pm 0.7 \mu\text{m}/\mu\text{m}^2$, significantly
554 larger ($p < 0.05$) than the value found for the MF-gel, $9.5 \pm 0.3 \mu\text{m}/\mu\text{m}^2$. The boundary length
555 per unit area values obtained for the gels were larger when the particle aggregate sizes were
556 smaller (Table 3). This result was expected because matrices with smaller particle aggregates
557 present more interfaces (particle aggregates/aqueous phase).

558 Values of boundary length per unit area were significantly larger ($p < 0.05$) in the gels
559 when compared to suspensions. This result was also expected because particle sizes in
560 suspensions were found to be significantly smaller ($p < 0.05$) than particle aggregate sizes in
561 gels. Therefore, in suspensions, more interfaces (particle/aqueous phase) were present,
562 resulting in bigger values of boundary length per unit area values.

563 Tortuosity values were similar for the two concentrated milk gels (1.5 ± 0.2 and $1.5 \pm$
564 0.2 for MF- and UF-gels, respectively). These values are much larger than for the
565 suspensions. This corresponds to the increase in the aggregate size, which leads to longer

566 paths between given points. In this study, the tortuosity value could not enable discrimination
567 between different gel microstructures but with similar casein composition.

568

569 **4. Conclusions**

570

571 An automated image analysis procedure for microstructural characterization of dairy
572 systems was developed. The procedure was first applied to models of synthetic suspensions,
573 and then on milk suspensions (with comparison with published data) to validate the
574 methodology. The computerized image analysis method enabled an easy measurement of a
575 series of microstructural parameters of milk gels, which makes it especially useful for routine
576 measurements.

577 The measurements of the area fraction (and hence of the sample porosity) were similar
578 for the MF- and UF-suspensions, and for the MF- and UF-gels. The image analysis procedure
579 made it possible to quantify differences of microstructure independently of the area fraction.
580 Binary image granulometry measures particle size distribution that can also be represented by
581 an average particle size. In a similar way, the distribution of distances between particles can
582 be represented by an average value. These two measurements can describe dairy systems by
583 using parameters that can be easily interpreted and compared.

584 The measurement of boundary length per unit area indicates the complexity of the
585 matrix microstructure, without making the assumption that the system is a collection of
586 particles. In case of particles systems with a similar area fraction, this parameter seems to be
587 correlated with the average particle size.

588 The tortuosity of a sample describes the complexity of the aqueous phase, and is
589 expected to be related to diffusion properties. In this study, the measured values were
590 different for suspensions and gels, but no difference could be discerned between the two gels

591 studied (obtained with different preparation methods). Tortuosity is difficult to measure when
592 the area fraction of the solid phase is large: when the aggregates are large, the probability of
593 observing non-connected aqueous phases increases. An alternative could be to allow the
594 computation of geodesic distances in both phases but using different propagation speeds (Wu
595 et al., 2006), or to consider the tortuosity over a limited distance.

596 It was demonstrated that the image analysis method for the estimation of
597 microstructural parameters was able to differentiate between dairy systems of similar
598 composition, but obtained from different processes.

599 For a better understanding of the microstructure of dairy systems, modeling
600 approaches might be considered. In this study, we have simulated binary images similar to
601 suspension images, with the objective of validating the image analysis methodology.
602 However, the microstructure of milk gels is much more complex and involves a variety of
603 physical and chemical processes. Several modeling approaches have already been undertaken
604 by other authors to reconstruct the microstructure based on 2D or 3D observations (Yeong &
605 Torquato, 1998; Kumar, Briant, & Curtin, 2006; Nisslert, Kvarnström, Loren, Nyden, &
606 Rudemo, 2007; Jiang, Chen, & Burkhart, 2013). Similar approaches could be investigated for
607 dairy systems.

608 The developed image analysis procedure enables new insights into the characterization
609 of the microstructure of dairy systems. This approach, which was applied to milk gels, might
610 be adapted and extended to other food systems.

611 This procedure can also contribute to a better understanding of the effects of
612 processing on the structure-property relationships in dairy products. For instance, further work
613 might focus on coupling measurements obtained by image analysis, which describe the
614 microstructure of milk gels, to physical phenomena such as diffusion properties.

615

616 **Acknowledgments**

617

618 The authors would like to thank Antoine Bouchoux (INSA, Toulouse, France) and
619 Marie-Hélène Famelart (INRA, Rennes, France) for their help and suggestions during the
620 writing of this paper. The authors also wish to thank the members of MRic TEM facility
621 (Rennes, France) for their help with the TEM observations. The authors acknowledge with
622 gratitude the financial support received both from the Brittany Regional Council and from
623 INRA Rennes (France).

624

References

- 625 Aguilera, J. M., Stanley, D. W., & Baker, K. M. (2000). New dimensions in microstructure of
626 food products. *Trends in Food Science & Technology*, 11(1), 3-9.
- 627 Aly, S., Floury, J., Famelart, M. H., Madec, M. N., Dupont, D., Le Gouar, Y. et al. (2011).
628 Nisin quantification by ELISA allows the modeling of its apparent diffusion
629 coefficient in model cheeses. *Journal of Agricultural and Food Chemistry*, 59(17),
630 9484-9490.
- 631 Andrey, P. & Maurin, Y. (2005). Free-D: an integrated environment for three-dimensional
632 reconstruction from serial sections. *Journal of Neuroscience Methods*, 145(1-2), 233-
633 244.
- 634 Anema, S. G. & Li, Y. (2003). Association of denatured whey proteins with casein micelles in
635 heated reconstituted skim milk and its effect on casein micelle size. *Journal of Dairy
636 Research*, 70, 73-83.
- 637 Bouchoux, A., Debbou, B., Gésan-Guiziou, G., Famelart, M.-H., & Doublier, J.-L. (2009).
638 Rheology and phase behavior of dense casein micelle dispersions. *The Journal of
639 Chemical Physics*, 131(16).
- 640 Büchheim, W. (1982). Aspects of sample preparation for freeze-fracture/freeze-etch studies of
641 proteins and lipids in food systems: a review. *Food Microstructure*, 1(2), 189-208.
- 642 Crossley, J. I. & Aguilera, J. M. (2001). Modeling the effect of microstructure on food
643 extraction. *Journal of Food Process Engineering*, 24(3), 161-177.
- 644 Dalgleish, D. G. & Corredig, M. (2012). The structure of the casein micelle of milk and its
645 changes during processing. *Annual Review of Food Science and Technology*, 3(1),
646 449-467.
- 647 Delarue, A. & Jeulin, D. (2003). 3D morphological characterization of composite materials
648 with spherical aggregates. *Image Analysis and Stereology*, 22, 153-161.
- 649 El-Bakry, M. & Sheehan, J. (2014). Analysing cheese microstructure: A review of recent
650 developments. *Journal of Food Engineering*, 125, 84-96.

- 651 Ercili-Cura, D., Lille, M., Legland, D., Gaucel, S., Poutanen, K., Partanen, R. et al. (2013).
652 Structural mechanisms leading to improved water retention in acid milk gels by use of
653 transglutaminase. *Food Hydrocolloids*, 30(1), 419-427.
- 654 Fallico, V., Tuminello, L., Pediliggieri, C., Horne, J., Carpino, S., & Licitra, G. (2006).
655 Proteolysis and microstructure of Piacentinu Ennese cheese made using different farm
656 technologies. *Journal of Dairy Science*, 89(1), 37-48.
- 657 Fenoul, F., Le Denmat, M., Hamdi, F., Cuvelier, G., & Michon, C. (2008). Technical Note:
658 Confocal Scanning Laser Microscopy and quantitative image analysis: Application to
659 cream cheese microstructure investigation. *Journal of Dairy Science*, 91(4), 1325-
660 1333.
- 661 Fox, P. F. & Brodtkorb, A. (2008). The casein micelle: Historical aspects, current concepts and
662 significance. *International Dairy Journal*, 18(7), 677-684.
- 663 Fucà, N., Pasta, C., Impoco, G., Caccamo, M., & Licitra, G. (2013). Microstructural
664 properties of milk fat globules. *International Dairy Journal*, 31(1), 44-50.
- 665 Geng, X. L., van den Berg, F. W. J., Bager, A. N., & Ipsen, R. (2011). Dynamic visualization
666 and microstructure of syneresis of cheese curd during mechanical treatment.
667 *International Dairy Journal*, 21(9), 711-717.
- 668 Goff, H. D., Verespej, E., & Smith, A. K. (1999). A study of fat and air structures in ice
669 cream. *International Dairy Journal*, 9(11), 817-829.
- 670 Gunasekaran, S. & Ding, K. (1999). Three-dimensional characteristics of fat globules in
671 cheddar cheese. *Journal of Dairy Science*, 82(9), 1890-1896.
- 672 Hussain, I., Grandison, A. S., & Bell, A. E. (2012). Effects of gelation temperature on
673 Mozzarella-type curd made from buffalo and cows milk. 1: Rheology and
674 microstructure. *Food Chemistry*, 134(3), 1500-1508.
- 675 Impoco, G., Carrato, S., Caccamo, M., & Tuminello, L. (2006). Quantitative analysis of
676 cheese microstructure using SEM imagery. In *SIMAI 2006 Minisymposium: Image*
677 *Analysis Methods for Industrial Application*.

- 678 Impoco, G., Fucà, N., Pasta, C., Caccamo, M., & Licitra, G. (2012). Quantitative analysis of
679 nanostructures shape and distribution in micrographs using image analysis. *Computers
680 and Electronics in Agriculture*, 84, 26-35.
- 681 Jeurnink, T. J. M. & de Kruif, K. G. (1993). Changes in milk on heating: viscosity
682 measurements. *Journal of Dairy Research*, 60(2), 139-150.
- 683 Jiang, G. Z., Chen, W., & Burkhart, C. (2013). Efficient 3D porous microstructure
684 reconstruction via Gaussian random field and hybrid optimization. *Journal of
685 Microscopy*, 252(2), 135-148.
- 686 Kalab, M., Allan-Wojtas, P., & Mistry, V. V. (1995). Microscopy and other imaging
687 techniques in food structure analysis. *Trends in Food Science & Technology*, 6, 3210-
688 3218.
- 689 Karlsson, A. O., Ipsen, R., Schrader, K., & Ardö, Y. (2005). Relationship between physical
690 properties of casein micelles and rheology of skim milk concentrate. *Journal of Dairy
691 Science*, 88(11), 3784-3797.
- 692 Kethireddipalli, P., Hill, A. R., & Dagleish, D. G. (2011). Interaction between casein micelles
693 and whey protein/kappa-casein complexes during renneting of heat-treated
694 reconstituted skim milk powder and casein micelle/serum mixtures. *Journal of
695 Agricultural and Food Chemistry*, 59(4), 1442-1448.
- 696 Kumar, H., Briant, C. L., & Curtin, W. A. (2006). Using microstructure reconstruction to
697 model mechanical behavior in complex microstructures. *Mechanics of Materials*,
698 38(8-10), 818-832.
- 699 Lanfrey, P. Y., Kuzeljevic, Z. V., & Dudukovic, M. P. (2010). Tortuosity model for fixed
700 beds randomly packed with identical particles. *Chemical Engineering Science*, 65(5),
701 1891-1896.
- 702 Latour, L. L., Kleinberg, R. L., Mitra, P. P., & Sotak, C. H. (1995). Pore-size distributions and
703 tortuosity in heterogeneous porous media. *Journal of Magnetic Resonance, Series A*,
704 112(1), 83-91.

- 705 Le Feunteun, S. & Mariette, F. (2007). Impact of casein gel microstructure on self-diffusion
706 coefficient of molecular probes measured by ^1H PFG-NMR. *Journal of Agricultural*
707 *and Food Chemistry*, 55(26), 10764-10772.
- 708 Le Feunteun, S. & Mariette, F. (2008). PFG-NMR techniques provide a new tool for
709 continuous investigation of the evolution of the casein gel microstructure after
710 renneting. *Macromolecules*, 41(6), 2071-2078.
- 711 Legland, D., Devaux, M. F., Bouchet, B., Guillon, F., & Lahaye, M. (2012). Cartography of
712 cell morphology in tomato pericarp at the fruit scale. *Journal of Microscopy*, 247(1),
713 78-93.
- 714 Legland, D., Kiêu, K., & Devaux, M. F. (2007). Computation of Minkowski measures on 2D
715 and 3D binary images. *Image Analysis and Stereology*, 26(6), 83-92.
- 716 Lucey, J. A. (2002). Formation and physical properties of milk protein gels. *Journal of Dairy*
717 *Science*, 85(2), 281-294.
- 718 Marchesseau, S., Gastaldi, E., Lagaude, A., & Cuq, J. L. (1997). Influence of pH on protein
719 interactions and microstructure of process cheese. *Journal of Dairy Science*, 80(8),
720 1483-1489.
- 721 Maubois, J. L. & Mocquot, G. (1971). Préparation de fromage à partir de "pré-fromage
722 liquide" obtenu par ultrafiltration du lait. *Lait*, 51(508), 495-533.
- 723 Maubois, J. L. & Mocquot, G. (1975). Application of membrane ultrafiltration to preparation
724 of various types of cheese. *Journal of Dairy Science*, 58(7), 1001-1007.
- 725 Maubois, J. L., Mocquot, G., & Vassal, L. (1969). A method for processing milk and milk
726 products. [2052121]. French.
- 727 McMahon, D. J., Fife, R. L., & Oberg, C. J. (1999). Water partitioning in Mozzarella cheese
728 and its relationship to cheese meltability. *Journal of Dairy Science*, 82(7), 1361-1369.
- 729 McMahon, D. J. & McManus, W. R. (1998). Rethinking casein micelle structure using
730 electron microscopy. *Journal of Dairy Science*, 81(11), 2985-2993.

- 731 Mellema, M., Heesakkers, J. W. M., van Opheusden, J. H. J., & van Vliet, T. (2000).
732 Structure and scaling behavior of aging rennet-induced casein gels examined by
733 confocal microscopy and permeametry. *Langmuir*, 16(17), 6847-6854.
- 734 Morand, M., Guyomarc'h, F., Legland, D., & Famelart, M. H. (2012). Changing the
735 isoelectric point of the heat-induced whey protein complexes affects the acid gelation
736 of skim milk. *International Dairy Journal*, 23(1), 9-17.
- 737 Nair, P. K., Dalgleish, D. G., & Corredig, M. (2013). Colloidal properties of concentrated
738 heated milk. *Soft Matter*, 9(14), 3815-3824.
- 739 Nisslert, R., Kvarnström, M., Loren, N., Nyden, M., & Rudemo, M. (2007). Identification of
740 the three-dimensional gel microstructure from transmission electron micrographs.
741 *Journal of Microscopy*, 225(1), 10-21.
- 742 Ohser, J. & Mücklich, F. (2000). *Statistical analysis of microstructures in materials sciences*.
743 (1th ed.). Chichester: John Wiley & Sons.
- 744 Ong, L., Dagastine, R. R., Kentish, S. E., & Gras, S. L. (2011). Microstructure of milk gel and
745 cheese curd observed using cryo scanning electron microscopy and confocal
746 microscopy. *Food Science and Technology*, 44(5), 1291-1302.
- 747 Ong, L., Dagastine, R. R., Kentish, S. E., & Gras, S. L. (2012). The effect of pH at renneting
748 on the microstructure, composition and texture of Cheddar cheese. *Food Research*
749 *International*, 48(1), 119-130.
- 750 Ong, L., Dagastine, R. R., Kentish, S. E., & Gras, S. L. (2013). The effect of calcium chloride
751 addition on the microstructure and composition of Cheddar cheese. *International*
752 *Dairy Journal*, 33(2), 135-141.
- 753 Otsu, N. (1979). A threshold selection method from gray-level histograms. *IEEE Transactions*
754 *on Systems, Man, and Cybernetics*, 9(1), 62-66.
- 755 Ramasubramanian, L., Webb, R., D'Arcy, B., & Deeth, H. C. (2013). Characteristics of a
756 calcium–milk coagulum. *Journal of Food Engineering*, 114(2), 147-152.
- 757 Reis, P. J. M. & Malcata, F. X. (2011). Ripening-related changes in Serra da Estrela cheese: A
758 stereological study. *Journal of Dairy Science*, 94(3), 1223-1238.

- 759 Rovira, S., Lopez, M. B., Ferrandini, E., & Laencina, J. (2011). Hot topic: Microstructure
760 quantification by scanning electron microscopy and image analysis of goat cheese
761 curd. *Journal of Dairy Science*, *94*(3), 1091-1097.
- 762 Sam Saguy, I., Marabi, A., & Wallach, R. (2005). New approach to model rehydration of dry
763 food particulates utilizing principles of liquid transport in porous media. *Trends in*
764 *Food Science & Technology*, *16*(11), 495-506.
- 765 Shen, L. & Chen, Z. (2007). Critical review of the impact of tortuosity on diffusion. *Chemical*
766 *Engineering Science*, *62*(14), 3748-3755.
- 767 Silva, J. V. C., Peixoto, P. D. S., Lortal, S., & Flourey, J. (2013). Transport phenomena in a
768 model cheese: The influence of the charge and shape of solutes on diffusion. *Journal*
769 *of Dairy Science*, *96*(10), 6186-6198.
- 770 Singh, H. & Waungana, A. (2001). Influence of heat treatment of milk on cheesemaking
771 properties. *International Dairy Journal*, *11*(4-7), 543-551.
- 772 Smith, A. K., Kakuda, Y., & Goff, H. D. (2000). Changes in protein and fat structure in
773 whipped cream caused by heat treatment and addition of stabilizer to the cream. *Food*
774 *Research International*, *33*(8), 697-706.
- 775 Soille, P. (2003). *Morphological Image Analysis: Principles and Applications*. (2 ed.).
776 Secaucus, NJ, USA: Springer-Verlag New York, Inc.
- 777 Srilaorkul, S., Ozimek, L., Oraikul, B., Hadziyev, D., & Wolfe, F. (1991). Effect of
778 ultrafiltration of skim milk on casein micelle size distribution in retentate. *Journal of*
779 *Dairy Science*, *74*(1), 50-57.
- 780 Suman, R. & Ruth, D. (1993). Formation factor and tortuosity of homogeneous porous media.
781 *Transp Porous Med*, *12*(2), 185-206.
- 782 Torquato, S. (2002). *Random heterogeneous materials: microstructure and macroscopic*
783 *properties*. New York: Springer-Verlag.
- 784 Ulve, V. M., Monnet, C., Valence, F., Fauquant, J., Falentin, H., & Lortal, S. (2008). RNA
785 extraction from cheese for analysis of in situ gene expression of *Lactococcus lactis*.
786 *Journal of Applied Microbiology*, *105*(5), 1327-1333.

- 787 Walstra, P., Bloomfield, V. A., Jason Wei, G., & Jenness, R. (1981). Effect of chymosin
788 action on the hydrodynamic diameter of casein micelles. *Biochimica et Biophysica*
789 *Acta (BBA) - Protein Structure*, 669(2), 258-259.
- 790 Waninge, R., Kalda, E., Paulsson, M., Nylander, T., & Bergenstahl, B. (2004). Cryo-TEM of
791 isolated milk fat globule membrane structures in cream. *Physical Chemistry and*
792 *Chemical Physics*, 6, 1518-1523.
- 793 Waninge, R., Nylander, T., Paulsson, M., & Bergenstahl, B. (2003). Milk membrane lipid
794 vesicle structures studied with cryo-TEM. *Colloids and Surfaces B: Biointerfaces*,
795 31(1-4), 257-264.
- 796 Waungana, A., Singh, H., & Bennett, R. J. (1996). Influence of denaturation and aggregation
797 of beta-lactoglobulin on rennet coagulation properties of skim milk and ultrafiltered
798 milk. *Food Research International*, 29(8), 715-721.
- 799 Wium, H., Pedersen, P. S., & Qvist, K. B. (2003). Effect of coagulation conditions on the
800 microstructure and the large deformation properties of fat-free Feta cheese made from
801 ultrafiltered milk. *Food Hydrocolloids*, 17(3), 287-296.
- 802 Wu, Y. S., van Vliet, L. J., Frijlink, H. W., & van der Voort Maarschalk, K. (2006). The
803 determination of relative path length as a measure for tortuosity in compacts using
804 image analysis. *European Journal of Pharmaceutical Sciences*, 28(5), 433-440.
- 805 Yeong, C. L. Y. & Torquato, S. (1998). Reconstructing random media. *Physical Review e*,
806 57(1), 495-506.
- 807 Zalc, J. M., Reyes, S. C., & Iglesia, E. (2004). The effects of diffusion mechanism and void
808 structure on transport rates and tortuosity factors in complex porous structures.
809 *Chemical Engineering Science*, 59(14), 2947-2960.

Table Captions**Table 1**

Composition of the MF and UF concentrates.

Table 2

Values of parameters characterizing the microstructure of two concentrated milk suspensions (MF- and UF-suspensions) obtained from image analysis on binary micrographs¹.

Table 3

Values of parameters characterizing the microstructure of two concentrated milk gels (MF- and UF-gels) obtained from image analysis on binary micrographs¹.

Figure Captions

Fig. 1. Schematic representation of the automated segmentation procedure. The original TEM micrograph (A) is divided by a background image (B) to obtain a normalized image (C). The protein network is enhanced using a black top-hat filter (D), and smoothed to remove acquisition noise (E). Gray level histogram of the image, showing two peaks corresponding to the dark and white phases (F). The application of the Otsu threshold results in a binary image showing the protein phase as black and the void (aqueous) phase as white (G).

Fig. 2. Generation of a synthetic suspension of micelles. (A) 3D representation of a sample of the system of spheres (red) together with the region corresponding to the thick section (blue). (B) Sample binary image obtained by the intersection of the thick section with the system of spheres, projected along the z direction.

Fig. 3. Schematic representation of the microstructural parameters determined for dairy systems (suspensions and gels) by the image morphological granulometry method.

Fig. 4. Graphical illustration of tortuosity through a given point in a synthetic binary structure, computed as the ratio of the shortest lengths to borders (dashed line) over the image width (black line).

Fig. 5. TEM micrographs of concentrated milk suspensions and gels at 20000x magnification. (A) MF-suspension; (B) UF-suspension; (C) MF-gel; (D) UF-gel.

Fig. 6. Representative segmented TEM micrographs (binarised images) of concentrated milk suspensions and the related gels. (A) MF-suspension; (B) UF-suspension; (C) MF-gel; (D) UF-gel. These binarised images correspond to the TEM micrographs showed in Fig. 4.

Fig. 7. Distribution of particle sizes in TEM micrographs of (A) MF-suspension and (B) UF-suspension; Distribution of inter-particle distances in TEM micrographs of (C) MF-suspension and (D) UF-suspension.

Fig. 8. Distribution of particle aggregate sizes in TEM micrographs of (A) MF-gel and (B) UF-gel; Distribution of inter-particle aggregate distances in TEM micrographs of (C) MF-gel and (D) UF-gel.

Product	Dry matter (g/kg)	Caseins (g/kg)	Whey proteins (g/kg)	Lactose and Minerals (g/kg)	Other (g/kg)
MF concentrate	196	130.3	4.4	60.1	1.6
UF concentrate	223	130.7	27.3	63.1	1.8

Parameter	MF-suspension	UF-suspension
Area fraction	0.34 ± 0.02	0.33 ± 0.01
Porosity	0.66 ± 0.02	0.67 ± 0.01
Boundary length per unit area ($\mu\text{m}/\mu\text{m}^2$)	13.3 ± 0.5	$12.1 \pm 0.2^*$
Particle size (nm)	88 ± 3	$99 \pm 4^*$
Inter-particle distance (nm)	123 ± 5	$132 \pm 2^*$
Tortuosity	1.08 ± 0.01	1.06 ± 0.01

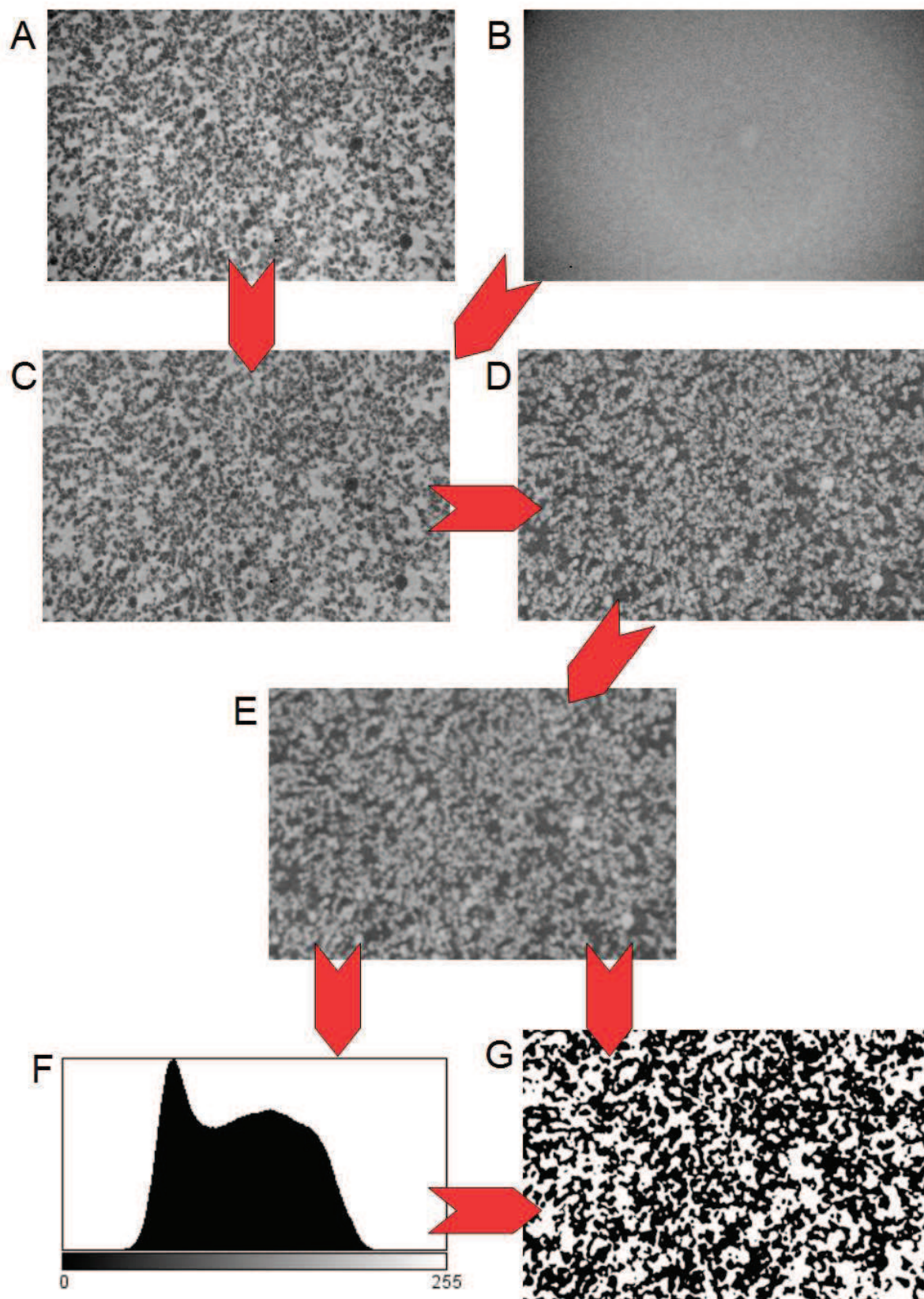
¹The results are expressed as the mean \pm standard deviation of the mean (n = 10).

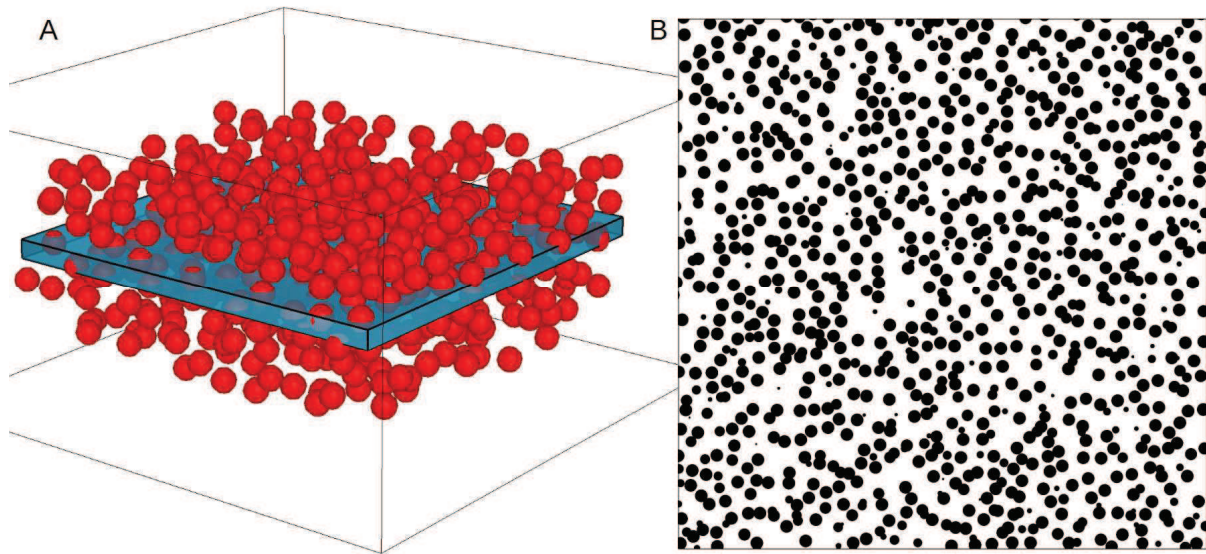
*The means within a single row are significantly different (p < 0.05).

Parameter	MF-gel	UF-gel
Area fraction	0.49 ± 0.03	0.50 ± 0.02
Porosity	0.51 ± 0.03	0.50 ± 0.02
Boundary length per unit area ($\mu\text{m}/\mu\text{m}^2$)	9.5 ± 0.3	10.7 ± 0.7*
Particle aggregate size (nm)	141 ± 3	135 ± 8*
Inter-particle aggregate distance (nm)	147 ± 5	131 ± 7*
Tortuosity	1.5 ± 0.2	1.5 ± 0.2

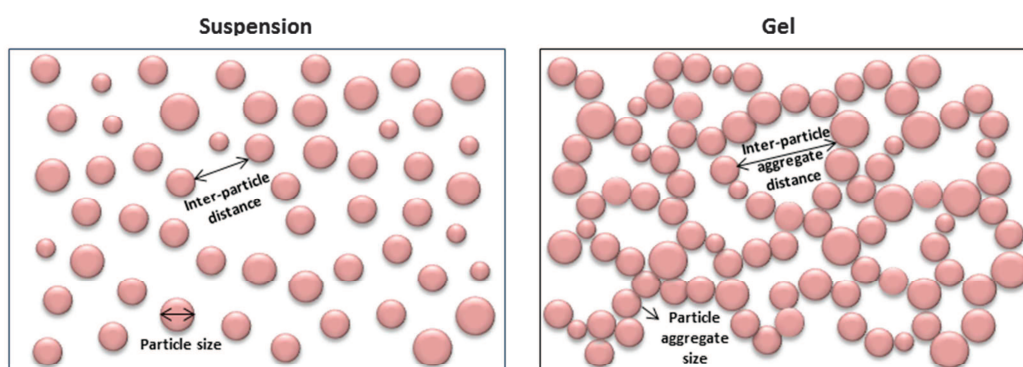
¹The results are expressed as the mean ± standard deviation of the mean (n = 10).

*The means within a single row are significantly different (p < 0.05).

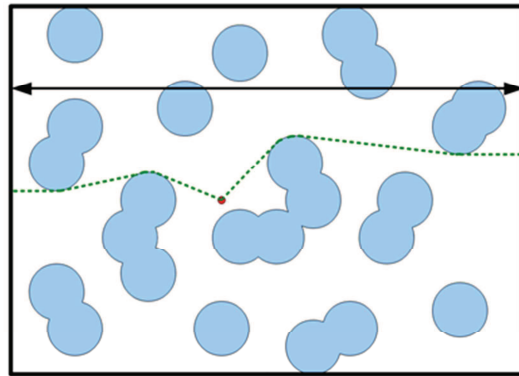




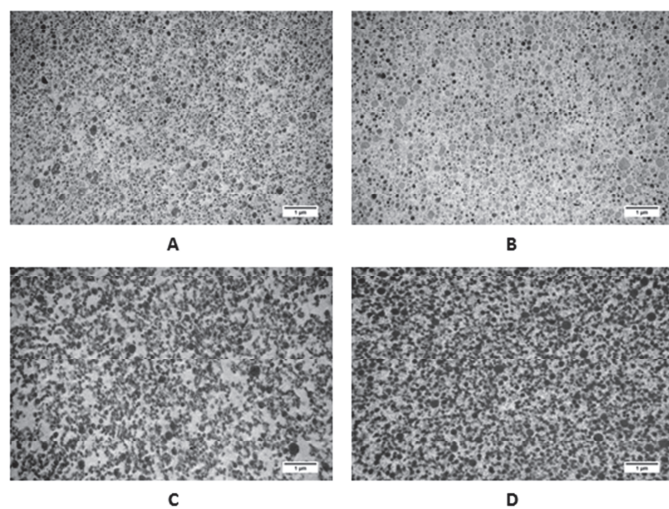
ACCEPTED MANUSCRIPT



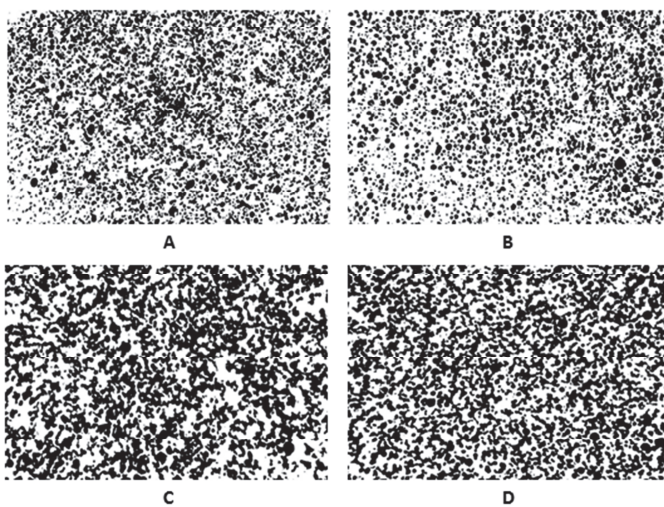
ACCEPTED MANUSCRIPT



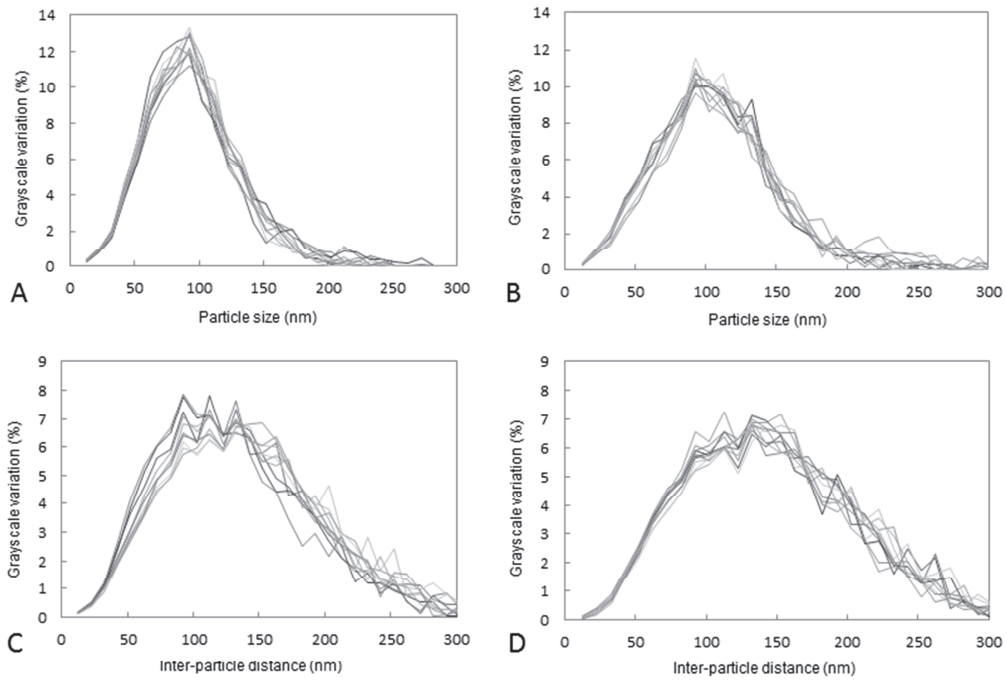
ACCEPTED MANUSCRIPT

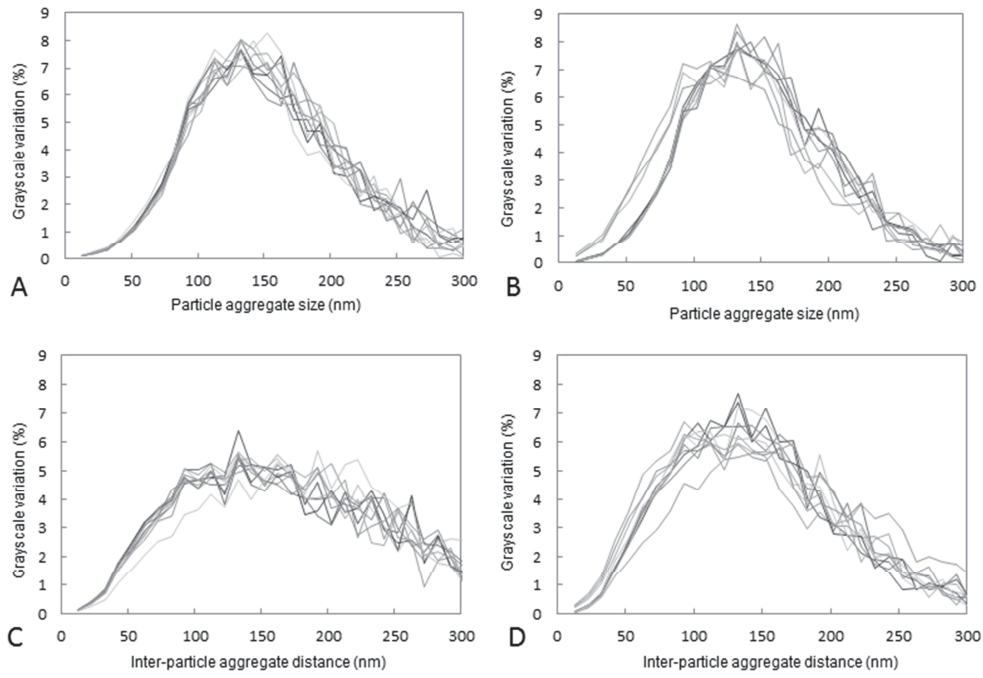


ACCEPTED MANUSCRIPT



ACCEPTED MANUSCRIPT





ACCEPTED MANUSCRIPT

Highlights

- We developed a method of characterization of the microstructure of dairy systems.
- Microstructural parameters were determined by an automated image analysis method.
- These routine measurements provided discrimination between different dairy systems.
- This method applied to milk gels can be easily transferred to other food systems.